Geochemical Perspectives Letters

^{190}Pt-^{186}Os geochronometer reveals open system behaviour of the ^{190}Pt-^{4}He isotope system

A. Luguet, G.M. Nowell, E. Pushkarev, C. Ballhaus, R. Wirth, A. Schreiber, I. Gottman

Supplementary Information

The Supplementary Information includes:

- 1. The Kondyor Zoned Ultramafic Complex (ZUC)
- 2. The Pt-alloys of the Kondyor ZUC and the Origin of their Pure Os Exsolution Lamellae
- 3. Methods
- Figure S-1
- Tables S-1 and S-2
- Supplementary Information References

1. The Kondyor Zoned Ultramafic Complex (ZUC)

The Kondyor ZUC is a circular, crater-like structure (*ca*. 6 km in diameter) having intruded the Archean basement and Proterozoic metasedimentary rocks of the Aldan Shield, on the SE edge of the Siberian Craton (*e.g*., Shcheka *et al*., 2004; Burg *et al*., 2009; Simonov *et al*., 2010) (Fig. S-1). Its zoned structure consists in a dunite core, the dominant rock type, surrounded by successive irregular shells of pyroxenites-wehrlites and gabbros and cross-cut in its SW part by numerous dykes of glimmerite, phlogopite-amphibole-apatite-carbonate and Fe-Ti-oxide bearing pyroxenites and magnetite-bearing clinopyroxenites (*e.g*., Burg *et al*., 2009). The platinum group minerals, namely Pt-alloys, are mostly associated with dm-sized chromite pods in the dunite. They render Kondyor one of the world's largest alluvial Pt deposits.

Neither the origin of the Kondyor ZUC (mantle intrusion at the apex of a mantle diapir; Burg *et al*., 2009 *vs*. fractional crystallisation of magma, see Simonov *et al*., 2010; Chaika and Izokh, 2018 for the Inagli Aldan ZUC) nor the age of the Pt mineralisation and the overall timeline of the Kondyor ZUC evolution are firmly constrained. Numerous investigations using the K-Ar, Rb-Sr, Sm-Nd isotopic systems on dunites, metasomatised dunites (*i.e*. phlogopite bearing), metasomatic pyroxenites-gabbros-syenites and late dykes at the whole-rock and mineral scales (*e.g*., phlogopite, clinopyroxene) indicate ages between 149-83 Ma (Orlova, 1992; Kononova *et al*., 1995; Pushkarev *et al*., 2002; Savatenkov and Mochalov, 2018), which are encompassing the "isochronal" ^{190}Pt-^{4}He age obtained on Pt-alloys (112 ± 7 Ma and 129 ± 6 Ma: Shukolyukov *et al*., 2012; Mochalov *et al*., 2016 respectively). In contrast, oval and rounded zircons from the dunitic core recorded Paleoproterozoic to Archean ages (1885 ± 52 and 2477 ± 18 Ma) (Malitch *et al*., 2012). Re-Os T_{RD} model ages obtained on (i) Pt-alloys and (ii) Os-alloys, erlichmanite (OsS_2), sperrylite ($PtAs_2$) associated with the Pt-alloys, collected from both the dunite-hosted chromitites and the placer deposit, point at Neoproterozoic (603-658 Ma) to future ages (Cabri *et al*., 1998; Malitch and Thalhammer, 2002) when back-calculated to the upper mantle ^{187}Os/^{188}Os estimate of Meisel *et al*. (2001).

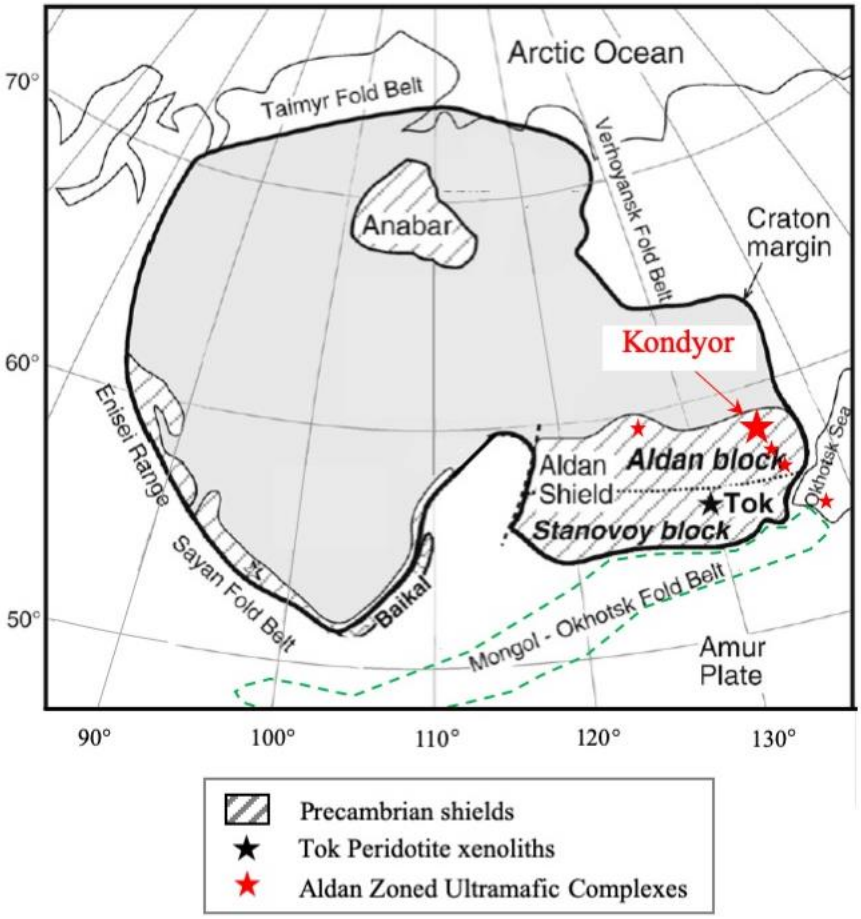

Figure S-1 Sketch map of the Siberian craton, the Aldan Shield and adjacent fold belts (modified from Tommasi *et al*., 2008).

2. The Pt-Alloys of the Kondyor ZUC and the Origin of their Pure Os Exsolution Lamellae

The Platinum Group Minerals of the Kondyor ZUC have been the focus of detailed investigations such as those of Malitch and Thalhammer (2002), Shcheka *et al*. (2004) and Nekrasov *et al*. (2005). The spectrum of Kondyor PGM is very wide consisting predominantly of Pt-alloys, mainly Pt_3Fe, with subordinate occurrences of Os±Ir±Ru alloys, sulfides of Highly Siderophile Elements (*e.g.*, laurite RuS_2, malanite $Cu(Pt, Ir)_2S_4$) and Pd-Pt compounds such as arsenides, tellurides, bismuthides and antimonites. The $^{190}Pt/^{188}Os$ and $^{187}Re/^{188}Os$ of our subset of Pt-alloys suggest that these Pt-alloys contain 10s ppm to wt. % Os and <100 ppb Re. Interestingly, the FIB-TEM investigations we conducted on a few grains revealed a very complex nanoscale exsolution pattern consisting of spinodal exsolutions of Pt-Fe alloys (*e.g.*, Pt_3Fe, PtFe) and pure Os exsolution lamellae (Fig. 1). Such nanoscale exsolution patterns were already observed by Malitch and Thalhammer (2002) and Shcheka *et al*. (2004).

Malitch and Thalhammer (2002) proposed that this mineralogical assemblage reflected a fractional crystallisation sequence starting at high temperature, low fS_2 conditions with the crystallisation of the Pt-Fe alloys, followed upon cooling and increasing fS_2-fO_2 by the exsolution of the Os lamellae, and the formation at lower temperature of the As, Te, Bi, Sn, Au, Cu, Pd, Pt compounds. Namely, the large Pt-alloys showing enrichments in Au-Ag-Cu-S-Sn-Sb-Bi-Te may have formed in a pegmatitic environment (*i.e.*, NaCl-rich solution) possibly generated when the residual liquids became fluid-saturated (Shcheka *et al*., 2004).

The $^{187}Os/^{188}Os$ signatures of the Kondyor Pt-alloys we obtained by LA-MC-ICPMS and especially their negative relationship with the $^{187}Re/^{188}Os$ ratios provide further insights into their origin(s) and the evolution of the Pt-mineralisation as a whole. The most unradiogenic $^{187}Os/^{188}Os$ composition of the Kondyor Pt-alloys (0.110096; grain D-S2), is obtained for the Os-poorest and Pt-

richest alloy (see ^{188}Os and $^{190}Pt/^{188}Os$: Table S-2) and reveals that the source of the Pt-mineralisation is likely an Archean mantle reservoir. In contrast, all the other analyses, which are clearly richer in Os, likely sampled a higher proportion of Os lamellae. These yield a much higher $^{187}Os/^{188}Os$ reaching up to ~0.1246 for the Os-richest alloy (grain E-S2). Considering the fractional crystallisation sequence proposed by Malitch and Thalhammer (2002), upon exsolution, the Os lamellae and their Pt-alloy hosts would have the same $^{187}Os/^{188}Os$ isotopic composition. Therefore, the most radiogenic $^{187}Os/^{188}Os$ of the Os exsolution-rich Pt-alloy (alloy E-S2) can only be explained due to ^{187}Os in-growth since the early Triassic mineralisation process if its Re/Os ratio is around 0.73 ($^{187}Re/^{188}Os$ ~ 3.5). Such a Re-rich composition is not supported by the EDS spectra of the Os exsolution lamellae (Fig. 1), nor by the $^{187}Re/^{188}Os$ ratios determined by LA-MC-ICPMS, nor the experimental investigations on Re and Os partitioning in HSE alloys of Fonseca *et al*. (2017). In fact, from both the natural PGM (see Walker *et al*., 1997; Meibom and Frei, 2002; Nowell *et al*., 2008b; Coggon *et al*., 2011; Wainwright *et al*., 2016) and experimental (Fonseca *et al*., 2017) viewpoints, it is expected that upon exsolution of pure Os lamellae from a Pt-alloy, the Re will partition preferentially into the Pt-Fe alloy while the Os will partition preferentially into the Os-alloys. Therefore, with ^{187}Os ingrowth, the more radiogenic $^{187}Os/^{188}Os$ signatures should develop within the Pt-Fe alloys, while the pure Os lamellae would be characterised by a lower, typically unradiogenic $^{187}Os/^{188}Os$ signature.

The Os-rich Pt-alloys (such as point E-S2) and the Os-poor Pt-alloy (grain D-S2), which can be found associated on the microscale within one single alloy grain (DS-1 and D-S2 in alloy grain D) represent thus different alloy generations or growth phases derived from mantle sources compositionally distinct. The shift from an Archean mantle source for the Os-poor Pt alloys to that of a mantle source characterised by a more radiogenic $^{187}Os/^{188}Os$ signatures for the Os-rich Pt-alloy, likely reflects the gradual overprinting of the Siberian cratonic mantle by subduction components over the ca. 100 millions years that the subduction of the Mongol-Okhotsk ocean seafloor lasted. The gradual overprinting by subduction components, namely fluids, is supported by the negative trend between $^{187}Os/^{188}Os$ *vs*. $^{187}Re/^{188}Os$ and the possible growth in pegmatitic environment of part of the PGM mineralogical assemblage suggested by Shcheka *et al*. (2004). The Kondyor Pt-alloys then possibly constitute an example where the overprinting event affected the mantle source of the Pt-mineralisation rather than purely affecting the alloys (*via* contamination and recrystallisation).

Such an alternative scenario for the evolution of the Kondyor Pt-alloys however requires to be firmly constrained by a thorough investigation at the micro to nanometric scale of the composition and isotopic signatures of the Os exsolution lamellae and their Pt-alloy hosts.

3. Methods

The simultaneous determination of the $^{187}Os/^{188}Os$ and $^{186}Os/^{188}Os$ signatures was performed by LA-MC-ICPMS using the New Wave UP213 nano-second laser system coupled with a Thermo-Finnigan Neptune MC-ICPMS of the Arthur Holmes Isotope Geology Laboratory at the Department of Earth Sciences of Durham, UK. The full details of the analytical procedure and data reduction are provided in Nowell *et al*. (2008b). Still, for the analytical session of the Kondyor Pt-alloys, the conditions of the laser system were specifically set to 20 Hz frequency, 100 % power and a 130 μm beam diameter. These laser conditions were kept constant throughout the analytical session allowing us to use the ^{188}Os signal as a proxy of the relative Os concentrations of the Kondyor alloys. Since the Kondyor alloys are Pt-rich and Os-poor, the mass bias correction for the whole analytical session was performed using the $^{189}Os/^{188}Os$ ratio (1.21978), as ^{189}Os is free from direct Pt interferences at the opposite of ^{192}Os or ^{190}Os.

The precision and accuracy of $^{186}Os/^{188}Os$ and $^{187}Os/^{188}Os$ ratios and the efficiency of the ^{187}Re and ^{186}W interference correction on the radiogenic ^{187}Os and ^{186}Os isotopes were estimated by measuring repetitively 1ppm DROsS standard solutions pure and variably doped in Re and W (by solution MC-ICPMS) as well as the Durham in-house Os-rich alloy standard (alloy grain 36720G3) (measured by LA-MC-ICPMS). The reproducibilities of the $^{186}Os/^{188}Os$ and $^{187}Os/^{188}Os$ compositions of the DROsS solutions (n=11, pure and, W- and Re-doped solutions) are respectively 96 ppm and 135 ppm. The $^{187}Os/^{188}Os$ variations are observed among as well as within the analyses of the pure, and of each of the W- and Re-doped solutions. These variations are then independent of the Re signal intensities, demonstrating that they do not result from a ^{187}Re interference correction issue. The reproducibility of the DROsS $^{186}Os/^{188}Os$ ratios improves significantly (33 ppm) when the analyses #1 and #2 from the pure DROsS solution are omitted. This combined to the absence of correlation between the ^{182}W beam intensity, the $^{182}W/^{188}Os$ and the $^{186}Os/^{188}Os$ demonstrates the robustness of the W-correction applied to W-bearing samples, with $^{182}W/^{188}Os$ ratios of up to 0.17 as seen for the 1ppm DROsS solution doped with 0.1 ppm W + 0.05 ppm Re. The Kondyor Pt-alloys show much lower $^{182}W/^{188}Os$ ratios (0.000004-0.0026), intermediate between those of the pure 1 ppm DROsS solution and the 1ppm solution doped with 0.05 ppm W and 0.01 ppm Re, for which the ^{186}W interference correction is robust.

Overall, our average DROsS $^{186}Os/^{188}Os$ and $^{187}Os/^{188}Os$ ratios differ by 207 ppm and 69 ppm when compared with those obtained on the pure 1 ppm DROsS standard solution (2.5 ppm) of Nowell *et al*. (2008a), and by 141 and 38 ppm when compared

with those obtained on the pure DROsS standard solution (0.2 ppm) of Nowell *et al*. (2008b). For the Durham in-house Os-rich alloy standard (alloy grain 36720G3), the $^{186}Os/^{188}Os$ and $^{187}Os/^{188}Os$ differ respectively by 195 ppm and 293 ppm when compared to the analyses of Nowell *et al*. (2008b) (see Table S-1) and show reproducibilities of 146 and 149 ppm respectively. The lower precision and accuracy obtained on the DROsS solutions and the alloy grain 36720G3 during the Kondyor analytical session most likely result from different analytical conditions (e.g., lower signal intensity by a factor 3.8 to 7.4). While these deviations are significant when the range of the $^{186}Os/^{188}Os$ signatures for the Earth's mantle is taken into consideration ($^{186}Os/^{188}Os$ variation of 95 ppm for ca. 3.5 Gyr), it is important to highlight that the range of $^{186}Os/^{188}Os$ and $^{187}Os/^{188}Os$ in the Kondyor Pt-alloys are 2-4 orders of magnitude larger than the precisions and accuracies estimated on our standard solutions and in-house standard Os-rich alloy.

Similarly to the procedure adopted in other publications investigating the $^{186}Os/^{188}Os$ of mantle samples (see Day *et al*., 2017), we have normalised our Kondyor Pt-alloys $^{186}Os/^{188}Os$ and $^{187}Os/^{188}Os$ ratios to the $^{186}Os/^{188}Os$ and $^{187}Os/^{188}Os$ ratios of standard materials in order to erase possible analytical bias. In doing so, we considered first the deviation between our average DROsS values obtained during the Kondyor analytical session and those determined on the 2.5 ppm DROsS solution by Nowell *et al*. (2008a). Importantly, all DROsS values used for this first normalisation are mass bias corrected using the $^{189}Os/^{188}Os$ ratios (1.21978) and measured by solution MC-ICPMS. We conducted a second normalisation as the interpretation of the $^{186}Os/^{188}Os$ and $^{187}Os/^{188}Os$ signatures of Kondyor Pt-alloys requires comparison to the $^{186}Os/^{188}Os$ and $^{187}Os/^{188}Os$ signatures of the primitive mantle (Day *et al*., 2017), these latter were estimated from TIMS analyses using $^{192}Os/^{188}Os$ as mass bias monitor. Such normalisation between TIMS, solution MC-ICPMS and LA-MC-ICPMS data and for different mass bias monitors is possible thanks to the extensive investigations performed on the $^{186}Os/^{188}Os$ and $^{187}Os/^{188}Os$ analytical procedure by Luguet *et al*. (2008-TIMS) and Nowell *et al*. (2008a, b-solution and LA-MC-ICPMS respectively), for which four standard solutions - available to cross-check the precision and accuracy of Os isotope measurements between laboratories - have been repetitively measured. This second normalisation is based on the deviations of the $^{186}Os/^{188}Os$ and the $^{187}Os/^{188}Os$ ratios for the UMd standard solution between the values obtained (i) by Nowell *et al*. (2008a) using solution-MC-ICPMS and $^{189}Os/^{188}Os$ for the bias correction and those determined by (ii) Day *et al*. (2017) using TIMS and $^{192}Os/^{188}Os$ for the mass bias correction.

These 2-fold normalisations only modify the values of the $^{186}Os/^{188}Os$ and $^{187}Os/^{188}Os$ signatures but do not alter any relationships that may exist between for example $^{190}Pt/^{188}Os$ and $^{186}Os/^{188}Os$ (*i.e.* isochron) or between $^{186}Os/^{188}Os$ vs. $^{187}Os/^{188}Os$. Finally, it is important to note that while this 2-fold normalisation of the $^{186}Os/^{188}Os$ and $^{187}Os/^{188}Os$ ratios allows for a direct comparison of datasets obtained by different laboratories using different analytical approaches and data reduction procedures (*i.e.* mass bias correction), the values of the $^{186}Os/^{188}Os$ and the $^{187}Os/^{188}Os$ obtained or normalised to match those obtained by TIMS may be slightly overestimated as the TIMS $^{186}Os/^{188}Os$ and $^{187}Os/^{188}Os$ data suffer from residual interferences (see Luguet *et al*., 2008).

Supplementary Tables

Table S-1 ^{188}Os, ^{182}W and ^{185}Re signal intensities and Os isotope compositions for the DROsS reference solution (Solution MC-ICPMS) and the Durham in-house Os-alloy standard 36720G3 (LA-MC-ICPMS) analysed during the analytical session of the Kondyor Pt-alloys.

Table S-1 (Part 1)

Analysis	^{188}Os(V)	1se	^{182}W (V)	1se	^{185}Re (V)	1se	$^{187}Re/^{188}Os$	1se
				DROsS solution				
				1 ppm DROsS				
#1	2.537	0.010	0.000034	0.000007	0.000042	0.000006	0.0000325	0.0000034
#2	2.686	0.007	0.000038	0.000004	0.000039	0.000004	0.0000236	0.0000020
#3	2.554	0.010	0.000030	0.000006	0.000042	0.000007	0.0000256	0.0000041
#4	2.546	0.009	0.000033	0.000005	0.000043	0.000006	0.0000265	0.0000033
#5	2.566	0.008	0.000027	0.000006	0.000050	0.000008	0.0000339	0.0000050
average #1-5							*0.000028*	
2 sd							*0.000009*	
				1 ppm DROsS + 0.05 ppm W + 0.01 ppm Re				
#6	2.837	0.009	0.245821	0.000775	0.091415	0.000286	0.055211	0.000006
#7	2.826	0.011	0.244571	0.000965	0.091062	0.000359	0.055204	0.000006
#8	2.809	0.015	0.243370	0.001305	0.090519	0.000486	0.055213	0.000005
average #6-8							*0.055209*	
2 sd							*0.000010*	
				1 ppm DROsS + 0.1 ppm W + 0.05 ppm Re				
#9	2.671	0.009	0.471057	0.001594	0.419768	0.001428	0.269247	0.000023
#10	2.679	0.009	0.472484	0.001541	0.421045	0.001355	0.269318	0.000019
#11	2.666	0.010	0.470179	0.001718	0.418942	0.001539	0.269295	0.000018
average #9-11							*0.269287*	
2 sd							*0.000073*	
average #1-11								
2 sd								
				Nowell *et al.* (2008a) 2.5 ppm DROsS (n=21)				
average								
2 sd								
				Nowell *et al.* (2008b) 0.2 ppm DROsS (n=5)				
average								
2 sd								
				Durham In-house standard 36720G3 Os-alloy				
#12	1.950	0.063	-0.000006	0.000005	0.001157	0.000029	0.001021	0.000009
#13	2.937	0.071	-0.000003	0.000006	0.001797	0.000054	0.001030	0.000008
#14	1.968	0.055	0.000001	0.000006	0.001273	0.000025	0.001118	0.000014
#15	1.507	0.050	-0.000002	0.000005	0.000931	0.000023	0.001065	0.000012
average #12-15								

2 sd								
Nowell *et al.* (2008b) (n=7)								
average	*11.11*							
2 sd	*2.05*							

Table S-1 (Part 2)

Analysis	$^{190}Pt/^{188}Os$	1se	$^{184}Os/^{188}Os$	1se	$^{186}Os/^{188}Os$	1se	$^{187}Os/^{188}Os$	1se
DROsS solution								
1 ppm DROsS								
#1	0.0000842	0.000050	0.001304	0.000004	0.119920	0.000008	0.160915	0.000006
#2	0.0000472	0.000027	0.001300	0.000002	0.119927	0.000003	0.160925	0.000003
#3	-0.0000473	0.000048	0.001308	0.000004	0.119937	0.000007	0.160927	0.000007
#4	-0.0000547	0.000052	0.001303	0.000003	0.119936	0.000007	0.160942	0.000007
#5	-0.0000324	0.000048	0.001308	0.000003	0.119937	0.000007	0.160924	0.000009
average #1-5	*-0.000001*		*0.001305*		*0.119931*		*0.160927*	
2 sd	*0.000125*		*0.000007*		*0.000015*		*0.000020*	
1 ppm DROsS + 0.05 ppm W + 0.01 ppm Re								
#6	0.000027	0.000048	0.001307	0.000007	0.119939	0.000005	0.160929	0.000006
#7	0.000034	0.000048	0.001314	0.000008	0.119936	0.000007	0.160928	0.000007
#8	-0.000070	0.000048	0.001308	0.000007	0.119937	0.000008	0.160937	0.000006
average #6-8	*-0.000003*		*0.001310*		*0.119937*		*0.160931*	
2 sd	*0.000116*		*0.000008*		*0.000002*		*0.000010*	
1 ppm DROsS + 0.1 ppm W + 0.05 ppm Re								
#9	0.000065	0.000045	0.001309	0.000011	0.119937	0.000010	0.160918	0.000013
#10	-0.000041	0.000052	0.001310	0.000013	0.119932	0.000013	0.160909	0.000012
#11	-0.000012	0.000046	0.001309	0.000009	0.119935	0.000013	0.160944	0.000012
average #9-11	*0.000004*		*0.001309*		*0.119935*		*0.160924*	
2 sd	*0.000110*		*0.000001*		*0.000005*		*0.000036*	
average #1-11	*0.000000*		*0.001307*		*0.119934*		*0.160927*	
2 sd	*0.000107*		*0.000008*		*0.000011*		*0.000022*	
Nowell *et al.* (2008a) 2.5 ppm DROsS (n=21)								
average			*0.001298*		*0.119909*		*0.160916*	
2 sd			*0.000002*		*0.000004*		*0.000004*	
Nowell *et al.* (2008b) 0.2 ppm DROsS (n=5)								
average					*0.119917*		*0.160921*	
2 sd					*0.000020*		*0.000018*	
Durham In-house standard 36720G3 Os-alloy								
#12	0.000277	0.000079	0.001305	0.000005	0.119844	0.000006	0.123950	0.000008
#13	-0.000049	0.000103	0.001301	0.000002	0.119845	0.000008	0.123952	0.000005
#14	0.000197	0.000108	0.001303	0.000004	0.119833	0.000010	0.123962	0.000009
#15	0.000112	0.000076	0.001310	0.000005	0.119827	0.000010	0.123970	0.000009

average #12-15	*0.000134*	*0.001305*	*0.119837*	*0.123958*
2 sd	*0.000279*	*0.000008*	*0.000017*	*0.000018*
Nowell *et al.* (2008b) (n=7)				
average	*0.000130*	*0.001305*	*0.119814*	*0.123922*
2 sd	*0.003280*	*0.000001*	*0.000009*	*0.000013*

Table S-2 ^{188}Os, ^{182}W and ^{185}Re signal intensities and Os isotope compositions of the Kondyor Pt-alloy grains (A to M) analysed by LA-MC-ICPMS.

Table S-2 (Part 1)

Alloy	^{188}Os(V)	1se	^{182}W (V)	1se	^{185}Re (V)	1se	^{187}Re/^{188}Os	1se
A-S1	0.356	0.042	0.000035	0.000006	0.000076	0.000006	0.000483	0.000055
A-S2	0.064	0.002	0.000021	0.000006	0.000049	0.000007	0.001271	0.000174
B-S1	0.145	0.002	0.000034	0.000007	0.000076	0.000005	0.000935	0.000058
B-S2	1.273	0.088	0.000040	0.000006	0.000070	0.000007	0.000100	0.000014
C-S1	0.379	0.022	0.000023	0.000005	0.000060	0.000006	0.000295	0.000029
C-S2	0.103	0.005	0.000033	0.000005	0.000067	0.000006	0.001233	0.000093
D-S1	0.192	0.016	0.000036	0.000006	0.000069	0.000006	0.000709	0.000075
D-S2	0.018	0.003	0.000047	0.000005	0.000035	0.000005	0.005411	0.001269
E-S1	0.142	0.003	0.000051	0.000006	0.000072	0.000006	0.000850	0.000075
E-S2	12.018	1.659	0.000048	0.000007	0.000110	0.000007	0.000046	0.000011
F-S1	0.729	0.145	0.000032	0.000005	0.000086	0.000005	0.000420	0.000051
F-S2	5.651	1.124	0.000069	0.000009	0.000088	0.000008	0.000250	0.000073
G-S1	2.750	0.552	0.000030	0.000005	0.000065	0.000006	0.000188	0.000035
G-S2	0.135	0.002	0.000027	0.000005	0.000057	0.000006	0.000677	0.000074
H-S1	0.150	0.008	0.000037	0.000005	0.000082	0.000006	0.000971	0.000082
H-S2	0.143	0.010	0.000036	0.000005	0.000071	0.000007	0.000910	0.000100
I-S1	0.526	0.048	0.000037	0.000004	0.000081	0.000008	0.000332	0.000037
I-S2	0.054	0.001	0.000024	0.000006	0.000076	0.000005	0.002320	0.000152
J-S1	0.135	0.002	0.000022	0.000006	0.000064	0.000006	0.000731	0.000059
J-S2	0.370	0.043	0.000041	0.000006	0.000069	0.000008	0.000424	0.000057
K-S1	0.143	0.001	0.000029	0.000005	0.000051	0.000006	0.000675	0.000067
K-S2	0.148	0.002	0.000043	0.000005	0.000059	0.000006	0.000722	0.000072
K-S3	0.136	0.002	0.000076	0.000053	0.000046	0.000006	0.000617	0.000079
K-S4	0.156	0.003	0.000042	0.000005	0.000067	0.000006	0.000759	0.000057
L-S1	0.083	0.002	0.000015	0.000006	0.000051	0.000006	0.000893	0.000108
L-S2	1.221	0.088	0.000016	0.000006	0.000044	0.000006	0.000069	0.000011
M-S1	0.616	0.156	0.000120	0.000071	0.000057	0.000007	0.000402	0.000073
M-S2	0.090	0.002	0.000022	0.000006	0.000044	0.000006	0.000793	0.000117

Table S-2 (Part 2)

Alloy	^{190}Pt/^{188}Os	1se	^{184}Os/^{188}Os	1se	^{186}Os/^{188}Os	1se	^{187}Os/^{188}Os	1se
A-S1	1.42	0.11	0.001358	0.000029	0.120311	0.000051	0.120969	0.000269
A-S2	3.16	0.10	0.001201	0.000128	0.121065	0.000139	0.119044	0.000283
B-S1	2.57	0.05	0.001447	0.000056	0.120872	0.000085	0.120758	0.000122
B-S2	0.28	0.03	0.001295	0.000009	0.119922	0.000018	0.124286	0.000060
C-S1	0.82	0.04	0.001336	0.000021	0.120138	0.000032	0.123799	0.000055
C-S2	3.13	0.08	0.001417	0.000081	0.120970	0.000079	0.121587	0.000138

D-S1	2.32	0.19	0.001331	0.000045	0.120668	0.000073	0.122697	0.000176
D-S2	19.89	2.07	0.001996	0.000949	0.126959	0.001221	0.110096	0.002136
E-S1	2.79	0.05	0.001302	0.000044	0.120778	0.000055	0.122572	0.000097
E-S2	0.06	0.04	0.001307	0.000005	0.119852	0.000018	0.124577	0.000026
F-S1	1.17	0.14	0.001366	0.000022	0.120221	0.000042	0.123925	0.000090
F-S2	0.76	0.21	0.001309	0.000038	0.120037	0.000080	0.124251	0.000123
G-S1	0.66	0.10	0.001288	0.000015	0.119953	0.000039	0.124261	0.000059
G-S2	2.58	0.05	0.001433	0.000065	0.120789	0.000062	0.123240	0.000101
H-S1	2.68	0.12	0.001400	0.000060	0.120886	0.000086	0.123263	0.000101
H-S2	2.59	0.16	0.001290	0.000065	0.120692	0.000093	0.123453	0.000117
I-S1	0.85	0.06	0.001313	0.000015	0.120122	0.000031	0.124259	0.000048
I-S2	5.22	0.11	0.001130	0.000145	0.121829	0.000132	0.122365	0.000243
J-S1	2.26	0.04	0.001418	0.000052	0.120637	0.000066	0.123605	0.000085
J-S2	1.47	0.12	0.001325	0.000041	0.120317	0.000061	0.124083	0.000068
K-S1	2.29	0.04	0.001448	0.000045	0.120737	0.000063	0.123759	0.000076
K-S2	2.22	0.03	0.001313	0.000059	0.120676	0.000044	0.123641	0.000071
K-S3	2.34	0.03	0.001455	0.000055	0.120765	0.000057	0.123743	0.000092
K-S4	2.40	0.05	0.001331	0.000048	0.120575	0.000060	0.123616	0.000070
L-S1	2.70	0.06	0.001522	0.000103	0.120823	0.000096	0.123837	0.000121
L-S2	0.23	0.02	0.001317	0.000010	0.119925	0.000018	0.124602	0.000015
M-S1	1.11	0.11	0.001336	0.000039	0.120186	0.000055	0.124199	0.000093
M-S2	2.53	0.11	0.001331	0.000080	0.120703	0.000116	0.123665	0.000144

Supplementary Information References

Burg, J.-P., Bodinier, J.-L., Gerya, T., Bedini, R.-M., Boudier, F., Dautria, J.-M., Prikhodko, V., Efimov, A., Pupier, E., Balanec, J.-L. (2009) Translithospheric Mantle Diapirism: Geological Evidence and Numerical Modelling of the Kondyor Zoned Ultramafic Complex (Russian Far-East). *Journal of Petrology* 50, 289-321.

Cabri, L.J., Stern, R.A., Czamanske, G.K. (1998) Osmium isotope measurements of the Pt-Fe alloy placer nuggets from the Konder Intrusion using a Shrimp II Ion Microprobe. *8th International Platinum Symposium Abstracts*, 55-58.

Chaika, I.F., Izokh, A.E. (2018) Dunites of the Inagli massif (Central Aldan), cumulates of lamproitic magma. *Russian Geology and Geophysics* 59, 1450-1460.

Coggon, J. A. Nowell, G.M., Pearson, D.G., Oberthuïr, T., Lorand, J.-P., Melcher, F., Parman, S.W. (2012) The 190Pt-186Os decay system applied to dating platinum-group element mineralization of the Bushveld Complex, South Africa. *Chemical Geology* 302-303, 48-60.

Day, J.M.D., Walker, R.J., Warren, J.M. (2017) ^{186}Os-^{187}Os and highly siderophile element abundance systematics of the mantle revealed by abyssal peridotites and Os-rich alloys. *Geochimica et Cosmochimica Acta* 200, 232-254.

Fonseca, R.O.C, Brückel, K., Bragagni, A., Leitzke, F.P., Speelmanns, I.M., Wainwirght, A.N. (2017). Fractionation of rhenium from osmium during noble metal alloy formation in association with sulfides: Implications for the interpretation of model ages in alloy-bearing magmatic rocks. *Geochimica et Cosmochimica Acta* 216, 184-200.

Kononova,V.A., Pervov,V.A., Bogatikov, O.A., Mus-Shumacher, U., Keller, I. (1995). Mesozoic potassic magmatism of the Central Aldan: Geodynamics and genesis. *Geotectonics* 29, 224-234.

Luguet, A., Nowell, G.M., Pearson, D.G. (2008). ^{184}Os/^{188}Os and ^{186}Os/^{188}Os measurements by negative thermal ionisation mass spectrometry (NTIMS): Effects of interfering element and mass fractionation corrections on data accuracy and precision. *Chemical Geology* 248, 342-362.

Malitch, K.N., Thalhammer, O.A.R. (2002) Pt–Fe nuggets derived from clinopyroxenite–dunite massifs, Russia: a structural, compositional and osmium-isotope study. *The Canadian Mineralogist* 40, 395-418.

Malitch, K.N., Efimov, A.A., Badanina, I.Yu. (2012) The Age of Kondyor Massif Dunites (Aldan Province, Russia): First U–Pb Isotopic Data. *Doklady Earth Sciences* 446, 1054-1058.

Nekrasov, I.Y., Lennikov, A.M., Zalishchak, B.L., Oktyabrsky, R.A., Ivanov, V.V., Sapin, V.I., Taskaev, V.I (2005) Composition variations in platinum-group minerals and gold, Konder alkaline-ultrabasic massif, Aldan Shield, Russia, *The Canadian Mineralogist* 43, 637-654.

Nowell, G.M., Luguet, A., Pearson, D.G., Horstwood, M.A. (2008a). Precise and accurate ^{186}Os/^{188}Os and ^{187}Os/^{188}Os measurements by Multi-Collector Plasma Ionisation Mass Spectrometry (MC-ICP-MS) part I: solution analyses. *Chemical Geology* 248, 363-393.

Nowell, G.M., Pearson, D.G., Parman, S.W., Luguet, A., and Hanski, E. (2008b) Precise and accurate ^{186}Os/^{188}Os and ^{187}Os/^{188}Os measurements by Multi-Collector Plasma Ionisation Mass Spectrometry, part II: The application of laser ablation MC-ICPMS to single-grain Pt-Os and Re-Os geochronology in platinum group alloy grains. *Chemical Geology* 248, 394-426.

Orlova, M. P. (1992). Geology and genesis of the Konder Massif. *Geology of the Pacific Ocean* 8, 120-132.

Pearson, D.G., Parman, S.W., Nowell, G.M. (2007) A link between large mantle melting events and continent growth seen in osmium isotopes. *Nature* 449, 202-205.

Pushkarev Yu.D., Kostoyanov, A.I., Orlova, M.P., Bogomolov, E.S. (2002): Peculiarities of the Rb-Sr, Sm-Nd, Re-Os and K-Ar isotope systems in the Kondyor massif: mantle substratum, enriched by PGE. *Regional geology and metallogeny* 16, 80-91 (in Russ.)

Savatenkov, V.M., Mochalov, A.G. (2018) Age and Sources of Dunite from the Konder Massif (Aldan Shield). *Doklady Earth Sciences* 482, 1331-1335

Shcheka, G.G., Lehmann, B., Gierth, E., Gömann, K., Wallianos, A. (2004) Macrocrystals of Pt–Fe alloy from the Kondyor PGE placer deposit, Khabarovskiy Kray, Russia: trace-element content, mineral inclusions and reaction assemblages. *The Canadian Mineralogist* 42, 601-617.

Shukolyukov, Yu.A., Yakubovich, O.V., Mochalov, A.G., Kotov, A.B., Sal'nikova, E.B., Yakovleva, S.Z., Korneev, S.I., Gorokhovskii, B.M. (2012) New Geochronometer for the Direct Isotopic Dating of Native Platinum Minerals (190Pt-4He Method). *Petrology* 20, 491-507.

Simonov, V.A., Prikhod'ko, V.S., Kovyazin, S.V., Tarnavsky, A.V. (2010) Crystallization Conditions of Dunites in the Konder Platiniferous Alkaline–Ultramafic Massif of the Southeastern Aldan Shield, *Russian Journal of Pacific Geology* 4, 429-440.

Tommasi, A., Vauchez, A., Ionov, D.A. (2008) Deformation, static recrystallization, and reactive melt transport in shallow subcontinental mantle xenoliths (Tok Cenozoic volcanic field, SE Siberia) *Earth and Planetary Science Letters* 272, 65–77.

Wainwright, A.N., Luguet, A., Schreiber, A., Fonseca, R.O.C., Nowell, G.M., Lorand, J.-P., Janney, P.E. (2016) Nanoscale variations in ^{187}Os isotopic compositions and HSE systematics in a Bultfontein peridotite. *Earth and Planetary Science Letters* 447, 61-70.